Calculation of Unsteady Flows in Turbomachinery Using the Linearized Euler Equations

Kenneth C. Hall*
United Technologies Research Center, East Hartford, Connecticut
and
Edward F. Crawley†
Massachusetts Institute of Technology, Cambridge, Massachusetts

A method for calculating unsteady flows in cascades is presented. The model, which is based on the linearized unsteady Euler equations, accounts for blade loading, blade geometry, shock motion, and wake motion. Assuming that the unsteadiness in the flow is small, the unsteady Euler equations are linearized about the mean flow to obtain a set of linear variable-coefficient equations that describe the small-amplitude harmonic motion of the fluid. These linear equations are discretized on a computational grid via a finite-volume operator and solved directly, subject to an appropriate set of linearized boundary conditions. An important feature of the present analysis is the use of shock fitting to determine steady and unsteady shock positions. Use of the Euler equations in conjunction with the Rankine-Hugoniot shock-jump conditions correctly models the generation of entropy and vorticity at shocks. Results of this method are presented for both channel and cascade flows. Unsteady flows produced by blade motion (the flutter problem) and incoming disturbances (the gust-response problem) are predicted. A comparison of the present unsteady flow predictions to those of semi-analytical and time-marching numerical methods shows good agreement. Furthermore, the linearized Euler method requires substantially less computational time than the time-marching procedures.

Introduction

THE flutter and forced response of blading is a recurring problem in the development of turbomachinery. To predict these aeroelastic phenomena requires a detailed understanding of unsteady transonic flows in cascades. To date, most of the theoretical investigations on unsteady cascade flows have been based on the assumption of isentropic and irrotational flow and, therefore, do not account for the production of steady and unsteady entropy and vorticity across shocks. This deficiency can produce, under certain circumstances, serious errors in the predicted unsteady pressure distribution, shock motions, and unsteady blade loading. A method for predicting unsteady flows based on the linearized Euler equations is presented in this paper. The method accounts for the production of steady and unsteady entropy and vorticity across shocks and, therefore, should predict unsteady transonic flows more accurately.

Theoretical research into unsteady flows in cascades has progressed steadily over the past three decades. The methods used can be roughly divided into three types: analytical methods, semi-analytical methods, and numerical methods. Whitehead[1] studied the unsteady flow of an incompressible fluid through a cascade of vibrating flat plate airfoils. In this model it is assumed that the mean flow is uniform and undeflected by the cascade. Unsteady vorticity is distributed along the airfoils and shed vorticity is convected along the wake. The bound vorticity is distributed such that the velocity due to the vorticity is equal to the upwash velocity on the airfoil surfaces, and the Kutta condition is satisfied. This model, however, fails to predict experimentally observed bending flutter. Later, Whitehead[2] extended his model to that of a cascade of flat plate airfoils for which the mean flow was not uniform but was deflected or turned by the cascade. This new model did predict bending flutter and showed the importance of steady loading on the unsteady pressure distributions on vibrating airfoils. Atassi and Akai[3,4] developed a model in which point singularities were distributed along the surface of a two-dimensional airfoil surface of finite camber and thickness. With this model they studied steady and unsteady incompressible flows through a cascade of thick cambered airfoils. Their results, like Whitehead's, showed the importance of the steady blade loading on the unsteady flow in the cascade.

Lane and Friedman,[5] Whitehead,[6] and Smith[7] all analyzed flat plate cascades vibrating in a uniform subsonic flow. With compressibility there is the added complication of acoustic modes and acoustic resonance. Under certain circumstances, acoustic waves will propagate away from the rotor unattenuated, whereas in other cases the waves will be cut off. Smith[7] performed experiments to validate his model. For unloaded cascades, the theory is successful in predicting the cutoff behavior and the amplitude of the acoustic waves. For steadily loaded cascades, the amplitudes of the acoustic waves are not as well predicted.

Several investigators[8-12] have studied the problem of a cascade of vibrating flat plate airfoils in a uniform supersonic flow that is axially subsonic. Although the solution techniques differ, the same governing differential equations and boundary conditions were studied. These models are extremely important since they identified the occurrence of unstalled supersonic torsional flutter in fan stages. Because they apply to lightly loaded cascades, however, the models do not predict bending flutter, which has been experimentally observed in loaded cascades. Bendiksen[13] later used a perturbation scheme to calculate the effects due to small amounts of thickness, camber, and angle of attack as well as shock motion, and demonstrated the important role of shock motion in flutter prediction. Goldstein, Braun, and Adamczyk[14] have proposed a model in which the steady flow is everywhere parallel but has a strong nonisentropic in-passage shock. Hence, although

Received Dec. 9, 1987; revision received June 27, 1988.

*Associate Research Engineer, Theoretical and Computational Fluid Dynamics; formerly Fannie and John Hertz Foundation Fellow and Research Assistant, Department of Aeronautics and Astronautics, Massachusetts Institute of Technology.

†Associate Professor, Department of Aeronautics and Astronautics.

there is no turning, the blades carry a steady load due to the pressure rise across the shock. Furthermore, the unsteady shock motion is accounted for as well as the vorticity and entropy generation at the shock. Using the strong in-passage shock model, bending flutter is predicted for reduced frequencies (based on chord) below about 0.6. This result is more in keeping with experimentally observed bending flutter in compressors operating at high back pressures.

The lesson learned from these analytical and semi-analytical models is clear. To model accurately the flow in a cascade, one should include the effects due to the steady blade loading. The camber and thickness of the airfoil as well as the presence of strong shocks in the flows need to be accounted for. To investigate subsonic flows, Verdon and Caspar[15] numerically determined the mean flow about a cascade of airfoils in subsonic flow using a potential analysis. The governing equations were obtained by linearizing the full potential equations about a mean flow resulting in the linearized unsteady full potential equations. The resulting linear variable-coefficient equations are solved numerically using a finite-difference approximation. The computed unsteady pressure distributions agree well with tests conducted by Carta[16] on a linear cascade of oscillating airfoils. Whitehead and Grant[17] performed a similar analysis but used finite elements to discretize the field equations. Later, Verdon and Caspar[18] extended their original model to handle transonic flows. To model the effect of shock motion, shock fitting was used. Whitehead[19] also extended his model to the transonic regime but used shock capturing to model the shock motion. Both models require some form of artificial viscosity to stabilize the calculations in the supersonic regions.

Several investigators have used time-marching schemes to analyze unsteady flows in turbomachinery. Ni and Sisto[20] used a time-marching Euler method to calculate the pressure loads on vibrating flat plate airfoils in compressible flow. Actually, the method can be considered a hybrid of the time-marching and harmonic techniques as the quantities that are time-marched are the harmonic flow variables. Recently, Giles[21,22] has developed an Euler time-marching method based on Ni's Lax-Wendroff method[23] to study wake/rotor interaction. The ability to handle unequal rotor/stator pitches is accomplished by inclining the computational plane in time. This allows the calculations to be performed in a single blade passage. This code offers the advantage that nonlinear, anharmonic flows can be modeled. For numerical stability, however, the time-integration step size used in the integration must be fairly small. The maximum allowable time step is governed by the so-called CFL number. Because of this restriction, the size of the time steps is limited roughly by the size of the smallest cell in the domain. Hence, for accurate resolution of the flow, the required computational times become quite large.

The present linearized Euler analysis incorporates the improved flow model of the Euler methods into the linearized harmonic framework of the linearized potential methods. Hence, the method is both accurate and efficient. The linearized Euler analysis is divided into two main parts. The first step is to determine the steady flow. In order to fully account for such effects as blade thickness, loading, and strong in-passage shocks, the unsteady Euler equations should be linearized about a proper mean flow, and so despite the fact that we are primarily interested in the unsteady behavior of the fluid, the steady flow will also have to be calculated. Because of the periodicity in a cascade, the flow can be computed in a single blade passage. Within this passage, the steady Euler equations are discretized on a computational grid using a conservative finite-volume operator. The discretized equations are solved subject to an appropriate set of boundary conditions using a Newton iteration procedure. With this procedure, the nonlinear Euler equations are transformed into a sequence of linear equations[24-26] that are solved directly using Gaussian elimination. The Newton iteration procedure is extremely efficient and usually converges within five to ten iterations.

Once the steady solution has been obtained, the unsteady flow is determined. The nonlinear time-dependent Euler equations are linearized about the steady solution to obtain the linearized unsteady equations. These equations are linear with variable coefficients and describe the small disturbance behavior of the flow. Since many unsteady flows of interest are periodic in time, the unsteady flow is assumed to be harmonic in time. Under this assumption, explicit time dependency is eliminated from the unsteady problem. As with the steady Euler equations, the unsteady flow is computed in a single blade passage; the equations are discretized on a computational grid using a finite-volume operator and then solved directly using Gaussian elimination.

An important feature of the present method is that steady and unsteady shocks and wakes are fitted rather than captured. Most CFD codes use shock capturing to model shocks. This usually means that some artificial viscosity is added to the scheme. The resulting captured shock is not a sharp discontinuity but is smeared over several grid points. The advantage to this approach is that shocks are automatically captured wherever they happen to be, but increased grid resolution is needed in the area of the shock to produce a good approximation to a jump discontinuity. Using shock fitting, the position of the shock is modeled explicitly with unsteady shock-jump conditions applied across the shock.[26-28] These conditions, like the Euler equations themselves, can be linearized to obtain a set of linearized shock-jump conditions. Furthermore, the jump conditions fully account for the production of unsteady entropy and vorticity through shocks. This is a major improvement over the current linearized full potential theories. In particular, the present method can easily handle choked flows and properly predicts a bounded shock displacement for low-frequency flows.

Theoretical Approach

Flowfield Description

In reality, both steady and unsteady flows in turbomachines are extremely complicated. The fluid is viscous and heat conducting and is most accurately described by the Navier-Stokes equations. However, if the Reynolds number is sufficiently high and separation does not occur, then the viscous and heat-transfer effects are confined to narrow regions near the airfoil surfaces and the wakes. Under these circumstances, the Euler equations are a good approximation to the behavior of the flow and, hence, are the basis of the present unsteady flow analysis.

The internal energy $\hat{e}$ of a gas is in general a complex function of the its state, but for an ideal gas with constant specific heats, $\hat{e} = (1/\gamma - 1)\hat{p}$ where $\hat{p}$ is the fluid static pressure and γ is the ratio of specific heats. Hence, under this assumption, the two-dimensional Euler equations can be expressed in conservative form as

$$\frac{\partial}{\partial t}\begin{bmatrix} \hat{\rho} \\ \hat{\rho}\hat{u} \\ \hat{\rho}\hat{v} \\ \dfrac{\hat{p}}{\gamma-1} + \dfrac{1}{2}\hat{\rho}(\hat{u}^2+\hat{v}^2) \end{bmatrix} + \frac{\partial}{\partial x}\begin{bmatrix} \hat{\rho}\hat{u} \\ \hat{\rho}\hat{u}^2+\hat{p} \\ \hat{\rho}\hat{u}\hat{v} \\ \dfrac{\gamma}{\gamma-1}\hat{p}\hat{u} + \dfrac{1}{2}\hat{\rho}\hat{u}(\hat{u}^2+\hat{v}^2) \end{bmatrix} + \frac{\partial}{\partial y}\begin{bmatrix} \hat{\rho}\hat{v} \\ \hat{\rho}\hat{u}\hat{v} \\ \hat{\rho}\hat{v}^2+\hat{p} \\ \dfrac{\gamma}{\gamma-1}\hat{p}\hat{v} + \dfrac{1}{2}\hat{\rho}\hat{v}(\hat{u}^2+\hat{v}^2) \end{bmatrix} = 0 \tag{1}$$

or in vector notation

$$\frac{\partial \hat{U}}{\partial t} + \frac{\partial \hat{F}}{\partial x} + \frac{\partial \hat{G}}{\partial y} = 0 \tag{2}$$

where $\hat{\rho}$, $\hat{u}$, and $\hat{v}$ are the static density, and the x and y components of velocity, respectively. These four equations represent the conservation of mass, x and y momentum, and energy, respectively.

The unsteady Euler equations are nonlinear and time dependent and, therefore, computationally difficult to solve. In many cases, however, the amplitude of the unsteadiness in the flow is small. Hence, as with previous linearized full-potential theories, the unsteady flow can be approximated as the sum of a mean or steady flow component and a small-disturbance unsteady component, i.e.,

$$\hat{\rho}(x,y,t) = \bar{\rho}(x,y) + \rho(x,y,t) \tag{3}$$

$$\hat{u}(x,y,t) = U(x,y) + u(x,y,t) \tag{4}$$

$$\hat{v}(x,y,t) = V(x,y) + v(x,y,t) \tag{5}$$

$$\hat{p}(x,y,t) = P(x,y) + p(x,y,t) \tag{6}$$

The small perturbation assumption is valid for flows where the unsteady perturbations are less than about 10% of the mean flow.[26]

Next, these expansions are substituted into the Euler equations [Eq. (1)]. Collecting terms of equal order and neglecting terms of higher order produce the equations for the steady and the unsteady flow quantities. The mean flow (zeroth-order) equations are given by

$$\frac{\partial \boldsymbol{F}}{\partial x} + \frac{\partial \boldsymbol{G}}{\partial y} = 0 \tag{7}$$

where

$$\boldsymbol{F} = \begin{bmatrix} \bar{\rho}U \\ \bar{\rho}U^2 + P \\ \bar{\rho}UV \\ \dfrac{\gamma}{\gamma-1}PU + \dfrac{1}{2}\bar{\rho}U(U^2+V^2) \end{bmatrix}$$

$$\boldsymbol{G} = \begin{bmatrix} \bar{\rho}V \\ \bar{\rho}UV \\ \bar{\rho}V^2 + P \\ \dfrac{\gamma}{\gamma-1}PV + \dfrac{1}{2}\bar{\rho}V(U^2+V^2) \end{bmatrix}$$

which are just the original conservation equations with time derivative terms set to zero. Note that Eq. (7) is nonlinear in the steady primitive variables. More interesting are the unsteady (first-order) perturbation equations, which are given by

$$\frac{\partial}{\partial t}\boldsymbol{B}_1\boldsymbol{u} + \frac{\partial}{\partial x}\boldsymbol{B}_2\boldsymbol{u} + \frac{\partial}{\partial y}\boldsymbol{B}_3\boldsymbol{u} = 0 \tag{8}$$

where the variable coefficient matrices are given by

$$\boldsymbol{B}_1 = \begin{bmatrix} 1 & 0 & 0 & 0 \\ U & \bar{\rho} & 0 & 0 \\ V & 0 & \bar{\rho} & 0 \\ \dfrac{1}{2}(U^2+V^2) & \bar{\rho}U & \bar{\rho}V & \dfrac{1}{\gamma-1} \end{bmatrix}$$

$$\boldsymbol{B}_2 = \begin{bmatrix} U & \bar{\rho} & 0 & 0 \\ U^2 & 2\bar{\rho}U & 0 & 1 \\ UV & \bar{\rho}V & \bar{\rho}U & 0 \\ \dfrac{1}{2}U(U^2+V^2) & \dfrac{\gamma}{\gamma-1}P + \dfrac{3}{2}\bar{\rho}U^2 + \dfrac{1}{2}\bar{\rho}V^2 & \bar{\rho}UV & \dfrac{\gamma U}{\gamma-1} \end{bmatrix}$$

$$\boldsymbol{B}_3 = \begin{bmatrix} V & 0 & \bar{\rho} & 0 \\ UV & \bar{\rho}V & \bar{\rho}U & 0 \\ V^2 & 0 & 2\bar{\rho}V & 1 \\ \dfrac{1}{2}V(U^2+V^2) & \bar{\rho}UV & \dfrac{\gamma}{\gamma-1}P + \dfrac{1}{2}\bar{\rho}U^2 + \dfrac{3}{2}\bar{\rho}V^2 & \dfrac{\gamma V}{\gamma-1} \end{bmatrix}$$

and $\boldsymbol{u}$ is the vector of perturbation variables $[\rho,u,v,p]^T$. These equations are nonlinear in the mean flow variables but linear in the perturbation variables. The mean flow components are known from the solution of Eq. (7). Hence, the matrices premultiplying the perturbation variables are known variable coefficient matrices. Note also that the perturbation equations are in so-called conservation form.

One could in principle time march the linearized Euler equations to obtain an unsteady solution to the Euler equations that would be valid for small deviations away from the mean flow. However, many flows of interest are harmonic in time. Furthermore, many flows that are not harmonic are periodic in time. For the latter case, the unsteady perturbation flow can be represented as a Fourier series where the fundamental frequency ω is $2\pi/T$. But since the first-order equations are linear, the behavior of each Fourier component can be analyzed individually, then summed together to form the total solution. Without loss of generality, the Fourier components will be analyzed term by term. Hence, we let

$$\rho(x,y,t) \rightarrow \rho(x,y)e^{j\omega t} \tag{9}$$

$$u(x,y,t) \rightarrow u(x,y)e^{j\omega t} \tag{10}$$

$$v(x,y,t) \rightarrow v(x,y)e^{j\omega t} \tag{11}$$

$$p(x,y,t) \rightarrow p(x,y)e^{j\omega t} \tag{12}$$

where the perturbation amplitude terms [i.e., $\rho(x,y)$, etc.] on the right-hand side are complex. Substitution of the harmonic assumption into the linearized Euler equations gives

$$j\omega\boldsymbol{B}_1\boldsymbol{u} + \frac{\partial}{\partial x}\boldsymbol{B}_2\boldsymbol{u} + \frac{\partial}{\partial y}\boldsymbol{B}_3\boldsymbol{u} = 0 \tag{13}$$

Thus, the explicit time dependence has been removed. The result is a set of linear variable-coefficient equations for each temporal frequency of interest.

With this description of the mean and unsteady flowfields in hand, we turn our attention to the specification of the boundary conditions. Shown in Fig. 1 are the five main boundary surfaces to be considered. They are the moving airfoils, the upstream periodic boundaries, the downstream wake slip lines, the upstream far-field boundary, and the downstream far-field boundary. Furthermore, if a shock occurs in the domain, a sixth internal boundary must be considered to connect the two regions of continuous flow upstream and downstream of the shock. The far-field and periodic boundaries are introduced so that the steady and unsteady flows can be analyzed in a single cascade passage of finite axial extent. The boundary conditions are similar to those used in current linearized potential analyses as described by Verdon et al.[29] and Verdon[30] but are extended to apply to the present Euler theory. In the next three sections, these boundary conditions will be considered.

Flow Tangency

To begin, consider the boundary condition for a solid airfoil moving through a fluid. Suppose the surface of the airfoil at any point in time is described by the position vector $\hat{\boldsymbol{R}}$. Then, the boundary condition (flow tangency) at the surface of the airfoil is

$$\hat{\boldsymbol{V}} \cdot \hat{\boldsymbol{n}} - \frac{\partial \hat{\boldsymbol{R}}}{\partial t} \cdot \hat{\boldsymbol{n}} = 0 \tag{14}$$

where $\hat{n}$ is the unit normal to the surface. This boundary condition simply states that there is no mass flux through the surface of the airfoil. Note further that the unit normal to the airfoil $\hat{n}$ is a function of the airfoil surface position vector $\hat{R}$. Hence, Eq. (14) is nonlinear.

To linearize the flow tangency boundary condition we assume that the airfoil surface position, like the field variables, can be represented as the sum of two components: one describing the mean location and the other a small perturbation from this location that is a function of time, i.e.,

$$\hat{R}(s,t) = R(s) + r(s,t) \tag{15}$$

where the airfoil surface vector $\hat{R}$ has been expressed as a function of the distance s along the surface of the airfoil. Then the unit normal $\hat{n}$ and unit tangent $\hat{\tau}$ at the moving airfoil surface are related to the corresponding mean unit vectors $\bar{n}$ and $\bar{\tau}$ and the perturbed surface position by

$$\hat{n} = \bar{n} - \bar{\tau}\frac{\partial r}{\partial s}\cdot\bar{n} \tag{16}$$

$$\hat{\tau} = \bar{\tau} + \bar{n}\frac{\partial r}{\partial s}\cdot\bar{n} \tag{17}$$

These expressions are asymptotically valid for small airfoil motions.

Substitution of the perturbation assumption for the motion of the airfoil surface and the primitive flow variables into the flow tangency condition [Eq. (14)] and collection of terms of equal order gives the zeroth-order (mean) and the first-order (linearized unsteady) boundary conditions. The mean flow boundary condition is given by

$$V\cdot\bar{n} = 0 \tag{18}$$

which is simply the usual steady flow tangency condition. The first-order unsteady boundary condition is

$$v\cdot\bar{n} = \frac{\partial r}{\partial t}\cdot\bar{n} + V\cdot\tau\frac{\partial r}{\partial s}\cdot\bar{n} \tag{19}$$

Equation (19) states that the upwash on the blades is composed of two components. The first is due simply to the velocity of the airfoil normal to its surface. The second term is due to the rotation of the airfoil. If the airfoil is immersed in a moving fluid, then an "injection" velocity is required due to the ramp effect of the rotated airfoil. It should be emphasized that Eq. (19) must be applied at the instantaneous position of the airfoil surface and not the mean location. This is a problem since the computational grid we use is fixed in space. Hence, an additional term is required to extrapolate this boundary condition from the instantaneous airfoil position to its mean position. As a result, the boundary condition at the mean surface is

$$v\cdot\bar{n} = \frac{\partial r}{\partial t}\cdot\bar{n} + V\cdot\tau\frac{\partial r}{\partial s}\cdot\bar{n} - r\cdot\nabla(V)\cdot\bar{n} \tag{20}$$

If the flow to be analyzed is harmonic, then the operator $\partial/\partial t$ is replaced by $j\omega$.

Flow Discontinuities

The Euler equations are nonlinear and admit so-called weak solutions. Weak solutions are those that are not everywhere differentiable but nonetheless satisfy the integral form of the conservation equations. The solutions for flows that contain shocks or wakes fall into this category. In real flows, shocks and wakes have some small but finite thickness. However, in the absence of viscosity, shocks and wakes are modeled as surfaces at which the flow variables are discontinuous. In this section, the so-called jump conditions that govern the behavior of the flow at these surfaces are developed. These jump conditions will, subsequently, be used to fit shocks and wakes in the steady and unsteady flow analyses.

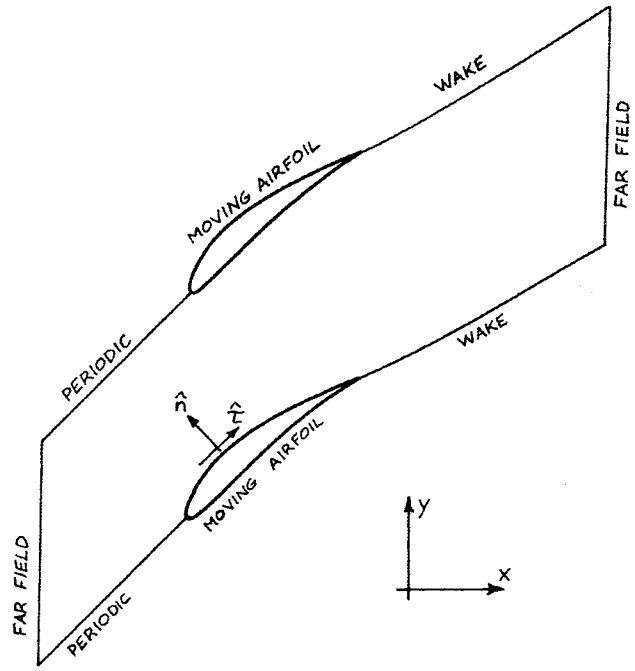

Fig. 1 Single cascade passage used for calculation of unsteady flows. Note five main boundary surfaces: moving airfoils, upstream periodic boundary, downstream periodic/wake slip-plane, upstream far-field boundary, and downstream far-field boundary.

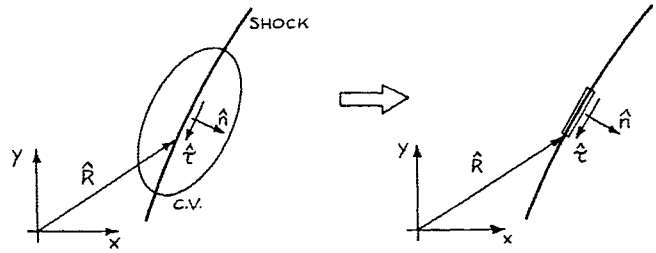

Fig. 2 Control volume used for the derivation of the shock jump conditions. The volume goes to zero in such a way that only a small length of the shock is enclosed.

The unsteady shock jump conditions are derived using the integral form of the conservation equations. Consider a volume D that contains a segment of a shock, as shown in Fig. 2. The shock position is described by the vector $\hat{R}$. The vectors $\hat{n}$ and $\hat{\tau}$ are the unit normal and the unit tangent to the shock surface, respectively. In general, the shock will not be stationary but will move through the fluid. Next, we imagine the surface S to shrink until it just encloses a small length of the shock. Evaluation of the integral form of the conservation equations results in a set of jump conditions that relate the flow on one side of a shock to the flow on the other. The conservation of mass, normal momentum, tangential momentum, and energy across the shock require that

$$\left[\!\left[\hat{\rho}\left(\hat{V} - \frac{\partial\hat{R}}{\partial t}\right)\cdot\hat{n}\right]\!\right] = 0 \tag{21}$$

$$\left[\!\left[\hat{p} + \hat{\rho}\hat{V}\cdot\hat{n}\left(\hat{V} - \frac{\partial\hat{R}}{\partial t}\right)\cdot\hat{n}\right]\!\right] = 0 \tag{22}$$

$$\left[\!\left[\hat{\rho}\hat{V}\cdot\tau\left(\hat{V} - \frac{\partial\hat{R}}{\partial t}\right)\cdot\hat{n}\right]\!\right] = 0 \tag{23}$$

$$\left[\!\left[\left(\frac{1}{\gamma-1}\hat{p} + \frac{1}{2}\hat{\rho}\hat{V}^2\right)\left(\hat{V} - \frac{\partial\hat{R}}{\partial t}\right)\cdot\hat{n} + \hat{p}\hat{V}\cdot\hat{n}\right]\!\right] = 0 \tag{24}$$

respectively, where the symbol $[\![\cdots]\!]$ denotes the difference in the enclosed quantity across a discontinuity. The tangential momentum shock-jump condition can be simplified further by using Eq. (21) to show that the jump in tangential velocity across the shock must be zero, i.e.,

$$[\![V \cdot \tau]\!] = 0 \tag{25}$$

Equations (21–25) are, of course, just the unsteady Rankine-Hugoniot relations that enable us to connect the two regions of continuous flow on either side of a shock. Note in particular the important role that the normal component of the shock velocity plays in the shock-jump conditions. In fact, the tangential component does not appear at all. Without much loss in generality, we may think of the motion of the shock as being normal to its surface. Alternatively, we may consider the shock to move in the direction of some arbitrary line (such as a computational grid line) so long as this line is not tangent to the shock.

Although the above jump conditions were derived for the case of a shock discontinuity, they are valid for any surface at which the flow variables are discontinuous. In particular, these jump conditions also apply to wakes. Unlike shocks, however, the wakes are surfaces of discontinuity through which mass does not flow; therefore, a flow tangency condition identical to the airfoil flow tangency condition applies at wake surfaces. Whereas the motion of the airfoils is prescribed, the wake motion must be determined as part of the solution. Because there is no mass flux through the wake, mass, tangential momentum, and energy are automatically conserved. The normal momentum jump condition reduces to the requirement that the pressure be continuous across the wake. Thus, the conditions to be applied at a wake surface are

$$\hat{V} \cdot \hat{n} = \frac{\partial \hat{R}}{\partial t} \cdot \hat{n} \tag{26}$$

$$[\![\hat{p}]\!] = 0 \tag{27}$$

Note that Eq. (26) must be applied on both sides of the wake. Hence, the pressure and the normal component of velocity are required to be continuous across a wake, whereas the tangential velocity and density, in general, will be discontinuous. One final requirement on the wake position is that the wake be attached to the trailing edge of the airfoil (for sharp trailing edges).

Like the Euler equations, the Rankine-Hugoniot conditions may be linearized to obtain the small disturbance behavior of the flow discontinuities. As in the linearization of the field equations, asymptotic series are used to represent the flow variables. As with the moving airfoil, the motion of the shock is described by a surface vector $\hat{R}$ that is composed of a mean plus an unsteady part. Substitution of the small disturbance assumptions for the shock displacement and the primitive fluid-dynamic variables into the nonlinear shock-jump conditions, and collection of terms of zeroth and first order gives the nonlinear mean and the linearized unsteady shock-jump conditions. The steady jump conditions are

$$[\![\bar{\rho} V \cdot \bar{n}]\!] = 0 \tag{28}$$

$$[\![P + \bar{\rho}\,(V \cdot \bar{n})^2]\!] = 0 \tag{29}$$

$$[\![V \cdot \bar{\tau}]\!] = 0 \tag{30}$$

$$\left[\!\!\left[\left(\frac{\gamma}{\gamma - 1} P + \frac{1}{2} \bar{\rho} V^2 \right) V \cdot \bar{n} \right]\!\!\right] = 0 \tag{31}$$

The linearized unsteady shock conditions are

$$\left[\!\!\left[\rho V \cdot \bar{n} + \bar{\rho} \left(v \cdot \bar{n} - V \cdot \bar{\tau} \frac{\partial r}{\partial s} \cdot \bar{n} - \frac{\partial r}{\partial t} \cdot n \right) + r \cdot \nabla (\bar{\rho} V) \cdot \bar{n} \right]\!\!\right] = 0 \tag{32}$$

$$\left[\!\!\left[p + \rho\,(V \cdot \bar{n})^2 + \bar{\rho} V \cdot \bar{n} \left(2v \cdot \bar{n} - 2V \cdot \bar{\tau} \frac{\partial r}{\partial s} \cdot \bar{n} - \frac{\partial r}{\partial t} \cdot n \right) + r \cdot \nabla [P + \bar{\rho} (V \cdot \bar{n})^2] \right]\!\!\right] = 0 \tag{33}$$

$$\left[\!\!\left[v \cdot \tau + V \cdot \bar{n} \frac{\partial r}{\partial s} \cdot \bar{n} + r \cdot \nabla (V) \cdot \bar{\tau} \right]\!\!\right] = 0 \tag{34}$$

$$\left[\!\!\left[\left(\frac{\gamma}{\gamma - 1} p + \frac{1}{2} \rho V^2 + \bar{\rho} V \cdot v \right) V \cdot \bar{n} + \left(\frac{\gamma}{\gamma - 1} P + \frac{1}{2} \bar{\rho} V^2 \right) \left(v \cdot \bar{n} - V \cdot \bar{\tau} \frac{\partial r}{\partial s} \cdot \bar{n} \right) - \left(\frac{1}{\gamma - 1} P + \frac{1}{2} \bar{\rho} V^2 \right) \frac{\partial r}{\partial t} \cdot \bar{n} + r \cdot \nabla \left[\left(\frac{\gamma}{\gamma - 1} P + \frac{1}{2} \bar{\rho} V^2 \right) V \right] \cdot \bar{n} \right]\!\!\right] = 0 \tag{35}$$

The terms proportional to $(\partial r / \partial s) \cdot \bar{n}$ arise from the rotation of the shock and, hence, the rotation of the unit normal and unit tangent vectors. The last term in each of these conditions extrapolates the jump conditions from the mean shock location to the instantaneous shock location. Therefore, the shock-jump conditions can be applied on a stationary grid through which the shock moves. The unknowns in Eqs. (32–35) are the magnitude of the shock displacement r and the perturbation variables ρ, u, v, and p on either side of the shock. The steady flow variables $\bar{\rho}$, U, V, and P are known from the solution of the steady flow problem. As with the linearized field equations, the time derivative operator $\partial / \partial t$ may be replaced by $j\omega$ if the flow is harmonic. As a rule of thumb, these linearized shock-jump conditions are a good approximation to the nonlinear conditions so long as the amplitude of the unsteady primitive variables is not more than 10% of the flow, the unsteady shock displacement is not more than about 10% of the typical length scale, and the shock does not move into a subsonic region.[26]

Similarly, the mean wake-jump conditions are given by

$$V \cdot \bar{n} = 0 \tag{36}$$

$$[\![P]\!] = 0 \tag{37}$$

The linearized unsteady wake-jump conditions are given by

$$v \cdot \bar{n} = \frac{\partial r}{\partial t} \cdot \bar{n} + V \cdot \bar{\tau} \frac{\partial r}{\partial s} \cdot \bar{n} - r \cdot \nabla (V) \cdot \bar{n} \tag{38}$$

$$[\![p + r \cdot \nabla P]\!] = 0 \tag{39}$$

Note the terms due to the rotation of the wake and the terms used to extrapolate from the mean wake location to the actual wake location. Equations (36) and (38) must be applied on both sides of the wake.

Far-Field Boundary Conditions

Because we will be solving for the unsteady flow in a cascade numerically, the computational domain cannot extend indefinitely in the axial direction. Usually, the computational domain will extend only about one chord length in front of the blade row. At this upstream boundary of the computational

domain, we need to apply an appropriate set of conditions that will allow unsteady disturbances to pass out of the domain without being reflected. The analysis below is somewhat similar to the characteristic boundary analysis used in time-marching schemes. In such schemes (unlike the present method), it is often assumed that any unsteady disturbances that impinge on the upstream boundary strike it with the wave fronts parallel to the boundary. That is, the partial derivative with respect to the tangential direction is negligible. This assumption results in the well-known one-dimensional characteristic boundary conditions. The characteristic variables represent vorticity, entropy, and two isentropic pressure waves. However, if the wave fronts are not parallel to the boundary, the wave will be partially reflected back into the computational domain. For steady-state calculations, this slows convergence. For unsteady flow calculations, this produces errors in the predicted unsteady flow quantities. Recently, several investigators have suggested higher-order nonreflecting boundary conditions that produce smaller reflections.[31-33] Fortunately, in the present analysis, exact nonreflecting boundary conditions can be imposed along the upstream boundary. This procedure, which is described below, is similar to the one used by Verdon et al.,[29] in their potential-flow analysis.

Consider the cascade passage shown in Fig. 1. Note that the x and y axes are aligned with the axial and tangential flow directions. We assume that sufficiently far upstream of the rotor the steady flow is uniform. Hence, the linearized Euler equations can be expressed as

$$\boldsymbol{B}_1 \frac{\partial \boldsymbol{u}}{\partial t} + \boldsymbol{B}_2 \frac{\partial \boldsymbol{u}}{\partial x} + \boldsymbol{B}_3 \frac{\partial \boldsymbol{u}}{\partial y} = 0 \tag{40}$$

Note that the matrices B_1, B_2, and B_3 appear outside of the differential operators due to the assumption of uniform mean flow.

The unsteady flowfield, whether due to an incoming gust or blade vibration, is assumed to have an interblade phase angle σ so that the solution has a spatial period in the tangential direction of $2\pi G/\sigma$ where G is the gap. For the analysis of the far field, it is convenient to represent the solution upstream of the rotor as a spatial Fourier series, i.e.,

$$\boldsymbol{u}(x,y,t) = \sum_{i=-\infty}^{\infty} \tilde{\boldsymbol{u}}_i e^{(j\omega t + j\beta_i y + jk_i x)} \tag{41}$$

where $\beta_i = (\sigma + 2\pi i)/G$, and k_i is a complex axial wave number to be determined. Substitution of Eq. (41) into Eq. (40) and collection of terms leads to

$$\sum_{i=-\infty}^{\infty} [\omega \boldsymbol{B}_1 + k_i \boldsymbol{B}_2 + \beta_i \boldsymbol{B}_3] \tilde{\boldsymbol{u}}_i e^{(j\omega t + j\beta_i y + jk_i x)} = 0 \tag{42}$$

For this equation to hold, each term of the infinite series must vanish. Hence,

$$[\omega \boldsymbol{B}_1 + k_i \boldsymbol{B}_2 + \beta_i \boldsymbol{B}_3] \tilde{\boldsymbol{u}}_i = 0 \tag{43}$$

Recall that ω and β_i are prescribed quantities. Equation (43) is then an eigenvalue problem for the eigenvalue k_i and the eigenvector $\tilde{\boldsymbol{u}}_i$. The eigenquantities are important since they determine the nature of the traveling waves and the speed and direction in which they travel. In particular, it can be shown that the so-called characteristic variables are directly related to the eigenvectors. To demonstrate this, we make a linear transformation from the four primitive variable Fourier coefficients $\tilde{\boldsymbol{u}}_i$ to the four characteristic variables $\tilde{\boldsymbol{w}}_i$, i.e.,

$$\tilde{\boldsymbol{u}}_i = \boldsymbol{T} \tilde{\boldsymbol{w}}_i \tag{44}$$

where $\boldsymbol{T}$ is chosen so as to diagonalize Eq. (43). That is to say, $\boldsymbol{T}$ is the matrix of right eigenvectors, and $\boldsymbol{T}^{-1}$ is the matrix of left eigenvectors. By solving this eigenvalue problem, it can be shown that the four characteristic variables are given by

$$\tilde{\boldsymbol{w}}_i = \boldsymbol{T}^{-1} \tilde{\boldsymbol{u}}_i \tag{45}$$

where

$$\boldsymbol{T}^{-1} = \begin{bmatrix} 0 & \beta_i V + \omega & -\beta_i U & -\dfrac{\sqrt{\beta_i^2(U^2+V^2-\bar{a}^2)+2\beta_i\omega V+\omega^2}}{\bar{\rho}\bar{a}} \\ 0 & \beta_i V + \omega & -\beta_i U & \dfrac{\sqrt{\beta_i^2(U^2+V^2-\bar{a}^2)+2\beta_i\omega V+\omega^2}}{\bar{\rho}\bar{a}} \\ 1 & 0 & 0 & -\dfrac{1}{\bar{a}^2} \\ 0 & \beta_i U & \beta_i V + \omega & \dfrac{\beta_i}{\bar{\rho}} \end{bmatrix}$$

The corresponding wave numbers are

$$k_{1i} = \frac{U(\omega + \beta_i V) + \bar{a}\sqrt{\beta_i^2(U^2+V^2-\bar{a}^2)+2\beta_i\omega V+\omega^2}}{U^2 - \bar{a}^2} \tag{46}$$

$$k_{2i} = \frac{U(\omega + \beta_i V) - \bar{a}\sqrt{\beta_i^2(U^2+V^2-\bar{a}^2)+2\beta_i\omega V+\omega^2}}{U^2 - \bar{a}^2} \tag{47}$$

$$k_{3i} = -\frac{\beta_i V + \omega}{U} \tag{48}$$

$$k_{4i} = -\frac{\beta_i V + \omega}{U} \tag{49}$$

The four characteristic variables represent the downstream and upstream moving pressure waves, an entropy wave, and a vorticity wave for the given tangential wave number β_i. The speed at which these waves propagate and the nature of their propagation are related to their respective axial wave numbers. If the wave number is real, then the wave propagates unattenuated. If the wave number is complex, then the wave will grow or decay in the x direction depending on the sign of the imaginary part. Note that the entropy and vorticity waves always propagate unattenuated, but the acoustic waves may or may not, depending on the conditions of the flow. If the conditions are such that the acoustic waves propagate, then the system is said to be superresonant. If the acoustic waves decay in the far field, then the system is said to be subresonant. The condition at which the waves just propagate is called acoustic resonance.[6,18]

If a wave propagates unattenuated, then its group velocity determines the direction that wave travels. Along the upstream boundary, the waves that enter the domain must be specified. If, on the other hand, the wave number is complex, then those waves that decay in the x direction are incoming waves and must be specified along the upstream boundary. For the flutter problem, this means that the incoming waves would be set to zero. For the gust response problem, the values of the characteristic variables would be chosen so as to model the incoming acoustic, entropic, and vortical waves. Analytically, the incoming waves corresponding to each tangential wave number β_i must be specified. Computationally, of course, only a finite number of tangential wave numbers are considered.

The application of the far-field boundary conditions downstream of the rotor is similar but is complicated by two factors. First, the unsteady flowfield is more complicated due to the presence of the unsteady wakes. This difficulty is removed by dividing the unsteady flowfield into a discontinuous part associated with the wake, and a continuous part that can be represented by a Fourier series. The far-field boundary conditions then are applied to this continuous part. Second, if the flow is transonic, shocks will in general cause the far downstream mean flow to be nonuniform in streamwise velocity and density. The solution is to use the average downstream properties in the far-field boundary conditions. Hence, for transonic flows, the downstream far-field condition is approximate. In any event, for subsonic outflow only one of the four characteristic variables (the upstream moving acoustic wave) is specified along the downstream boundary.

Numerical Model

In the previous section, the description of the unsteady flowfield has been reduced to a set of linear variable coefficient equations. In this section, the numerical technique used to solve these equations will be discussed.

For the present study, the computational grids used are logically rectangular and composed of quadrilateral conservation cells. The values of the mean flow and linearized unsteady primitive variables are stored at the corners of the conservation cells. At each of these cells, the linearized equations are discretized using a finite-volume operator similar to the one used by Ni.[23] The starting point is the linearized unsteady Euler equations in differential form [Eq. (13)]. If these equations hold over an entire conservation cell, then the integral over the cell must also be zero. Hence

$$\int\int \left(j\omega \boldsymbol{B}_1 \boldsymbol{u} + \frac{\partial}{\partial x} \boldsymbol{B}_2 \boldsymbol{u} + \frac{\partial}{\partial y} \boldsymbol{B}_3 \boldsymbol{u} \right) \mathrm{d}x\, \mathrm{d}y = 0 \tag{50}$$

Application of the divergence theorem yields the result

$$\int\int j\omega \boldsymbol{B}_1 \boldsymbol{u}\, \mathrm{d}x\, \mathrm{d}y + \oint (\boldsymbol{B}_2 \boldsymbol{u},\ \boldsymbol{B}_3 \boldsymbol{u}) \cdot \boldsymbol{n}\, \mathrm{d}s = 0 \tag{51}$$

The next step is to numerically approximate these integrals. The line integral can be evaluated using a trapezoidal integration around the cell, whereas the area integral is approximated by the average value of the integrand at the four corner nodes multiplied by the area of the conservation cell. This discretization scheme is second-order accurate. Furthermore, because the scheme is node-centered, no extrapolation to the boundaries is required to apply the boundary conditions. The major flaw with the scheme is that it admits sawtooth or hourglass modes. To eliminate such modes, a small amount of smoothing must be added to the scheme. The addition of smoothing is not totally undesirable, as some smoothing is needed to stabilize the solution at the sonic line for transonic problems. Regardless, very small amounts of smoothing are required in practice, but not enough to significantly alter the solution.

The boundary conditions and shock- and wake-jump conditions are discretized in a straightforward manner using second-order-difference operators. At shocks (or wakes), a double grid line is employed with upstream and downstream (or upper and lower) values of the primitive variable stored along these grid lines. An additional variable is introduced along these double grid lines that represents the local shock (or wake) displacement. Assembling the discretized field equations, boundary conditions, and jump conditions results in a large sparse linear system of equations whose solution gives the numerical approximation of the unsteady flow and the unsteady wake and shock displacements. In the present work, this system was solved using a banded Gaussian elimination solver.

Although the main objective of this effort is to predict unsteady flow phenomena, the mean flow must always be found before the unsteady analysis is performed. Preferably, this mean flow analysis should use wake and shock fitting, rather than the more conventional wake and shock capturing, so that accurate steady flow discontinuities will be available for use with the unsteady jump conditions. Early in this investigation, the decision was made to develop a steady solver based on the Newton iteration technique. The Newton iteration method for solving two-dimensional partial differential equations is an extremely fast algorithm.[24,25] Furthermore, the method reduces the nonlinear steady Euler equations to a series of linear ones, each of which is similar to the linearized unsteady Euler equations. This similarity greatly reduces the effort required to write both a mean flow and unsteady flow solver.

Consider the steady Euler equations [Eq. (7)] and suppose that an estimate of the actual solution is known. Then, the exact solution, or at least a much improved estimate, is assumed to be given by

$$\hat{\rho}(x,y) = \bar{\rho}(x,y) + \rho(x,y) \tag{52}$$

$$\hat{u}(x,y) = U(x,y) + u(x,y) \tag{53}$$

$$\hat{v}(x,y) = V(x,y) + v(x,y) \tag{54}$$

$$\hat{p}(x,y) = P(x,y) + p(x,y) \tag{55}$$

where the left-hand side is the improved estimate of the mean flow solution. The two terms on the right-hand side are the current estimate and the correction, respectively, where the correction is assumed to be small compared to the current estimate. After substituting Eqs. (52–55) into the steady Euler equations, expanding the result in a power series, and truncating second- and higher-order terms, we find that

$$\frac{\partial}{\partial x} \boldsymbol{B}_2 \boldsymbol{u} + \frac{\partial}{\partial y} \boldsymbol{B}_3 \boldsymbol{u} = -\left(\frac{\partial \boldsymbol{F}}{\partial x} + \frac{\partial \boldsymbol{G}}{\partial y} \right) \tag{56}$$

where $\boldsymbol{u}$ is the vector of corrections. The term on the right-hand side is the residuals of the steady Euler equations based on the current estimate of the flow. The left-hand side represents the first-order effect the correction perturbations have on the residuals. The variable coefficient matrices in Eq. (56) are identical to those in Eq. (13). The main differences between Eqs. (56) and (13) are that the linearized unsteady equations contain a homogeneous time-derivative term, whereas the Newton iteration equation contains an inhomogeneous residual term. In a similar way, the steady boundary conditions and jump conditions also can be linearized to obtain corresponding linearized conditions similar to their unsteady equivalents.

The basic Newton iteration procedure is then as follows. The procedure is started by making a reasonable guess for the steady flow solution including the locations of any shocks and wakes. The linearized steady Euler equations, the linearized steady jump conditions, and the linearized steady boundary conditions then are discretized on a computational grid in much the same way that the unsteady equations are. This linear set of equations then is solved by Gaussian elimination to determine the corrections and changes in the shock and wake positions. These corrections then are added to the current estimate of the solution to obtain an improved estimate. The grid then is modified so that the new shock and wake positions coincide with their double grid lines. The entire process is repeated until a converged solution is obtained. For subsonic flows, convergence usually occurs after only about five iterations. For transonic flow predictions, the procedure usually converges within five to ten iterations, although a poor initial guess for the solution can cause the procedure to diverge.

Discussion of Results

The first test case to be considered here is the flow through a hyperbolic channel. The steady subsonic transonic flow through this geometry was studied by Emmons[34,35] in the mid-1940's by using a stream function formulation solved via a relaxation technique. This geometry was selected here because the flow is highly two-dimensional, i.e., there is significant variation in flow properties across the width of the channel. Hence, if a shock occurs, it will be curved because of the highly two-dimensional flowfield. As such, the hyperbolic channel flow provides a good test case with which to evaluate the mean and unsteady shock-modeling capabilities of the present method.

The mean flow through the channel is determined by the inlet and exit conditions. The total pressure and total density at the inlet are specified to be unity. The downstream static pressure is set to 0.85. At this back pressure, the flow will be choked. The flow becomes supersonic as it passes through the throat and "shocks down" aft of the throat. A fairly coarse grid (33 × 9 nodes) was used to compute the steady and un-

steady solutions. Figure 3 shows the computed mean flow total pressure contours and the Mach number contours in the channel. For this example, about five Newton iterations were required to obtain a converged solution. Note that ahead of the shock where the flow is isentropic, the total pressure is constant. Downstream, however, there is some total pressure loss due to the production of entropy at the shock. The contours of total density are aligned with the local streamlines. Note the gradient in the total pressure as one moves from the lower wall toward the upper wall. This gradient appears because the shock strength varies from one side of the channel to the other. The inflow Mach number at the shock is large at the top of the channel and, hence, the shock is stronger resulting in a larger total pressure loss. Note further that the shock is normal to the wall at both the upper and lower walls.

Having computed the mean flow in the channel, the linearized unsteady Euler analysis is used to compute the unsteady flow. For this example, the complex amplitude of the inlet total pressure perturbation is set to unity, while the total density perturbation is set to 0.714 corresponding to an isentropic density variation. The excitation frequency is 2.0 corresponding to a reduced frequency $\bar{\omega}$ of 4.655 based on the channel length and sonic speed. Downstream, the static pressure is held constant; i.e., the unsteady pressure is zero. Note that these boundary conditions are reflecting; i.e., waves moving downstream will reflect off the exit boundary, sending acoustic waves upstream through the channel. The calculated unsteady pressure distribution along the lower channel wall is shown in Fig. 4. Note the jump discontinuity in the unsteady pressure at the shock. Figure 5 shows the unsteady shock motion. Shown is the shock position at four different times in one complete cycle. Note three important features of the shock motion. First, the shock remains normal to the wall at all times. Second, the upper part of the shock does not move as far as the lower part of the shock. The shock is stronger at the upper wall, and it must move through higher Mach number gradients. Hence, larger levels of unsteady entropy are generated per unit shock displacement along the upper wall, which tends to restrict the motion of the shock. Third, the upper part of the shock leads the lower part. This is a slightly more complicated feature. Along the upper wall ahead of the shock, the Mach number tends to be higher than along the lower wall. This means that the forward-moving pressure and convection waves tend to arrive at the shock earlier at the upper part of the shock. Similarly, downstream of the shock, because of the higher total pressure loss along the upper wall, the backward moving pressure wave moves faster along the upper wall than along the lower. Hence, any waves that are reflected off of the rear computational plane will arrive at the upper part of the shock more quickly than at the lower part. Both effects tend to cause the upper part of the shock to lead the lower portion.

The foregoing results demonstrate clearly some of the advantages of the present Euler analysis. First of all, there is no difficulty in predicting choked mean flow solutions. The back pressure uniquely fixes the shock location. Such cases are difficult to analyze using isentropic potential methods. Usually, the less physical "back potential" is specified and is adjusted until the shock is in the desired location.[36] Second, the use of shock fitting allows for an accurate representation of the shock position using fairly coarse grids. This significantly reduces the computational time required to solve transonic flow problems. Finally, although not demonstrated in the above example, the shock motion at low frequencies is correctly modeled. Tests similar to this one have shown that the linearized Euler analysis correctly predicts a finite-shock motion in the limit of low-frequency excitation, whereas a linearized potential analysis predicts an infinite-shock excursion.

The next flow to be considered is that through a cascade of Joukowski airfoils. The steady incompressible flow through this two-dimensional cascade has been examined previously by

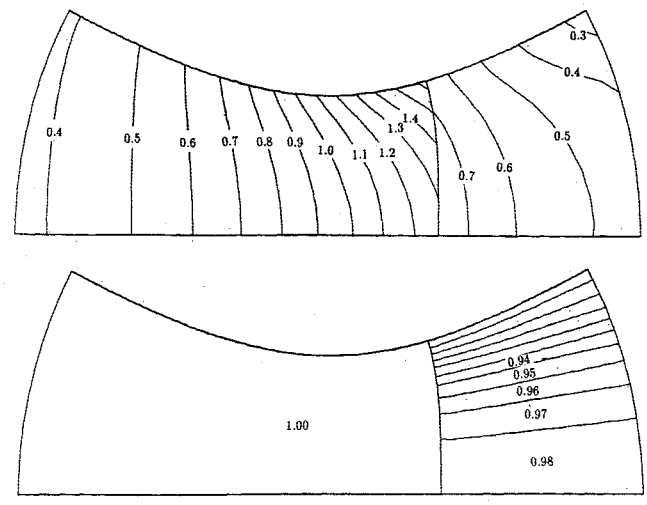

Fig. 3 Mach number and total pressure contours in choked hyperbolic channel. Note approximate grid resolution. Ahead of the shock the total pressure is constant. Downstream, lines of constant total pressure follow streamlines. The shock is strongest along upper channel wall.

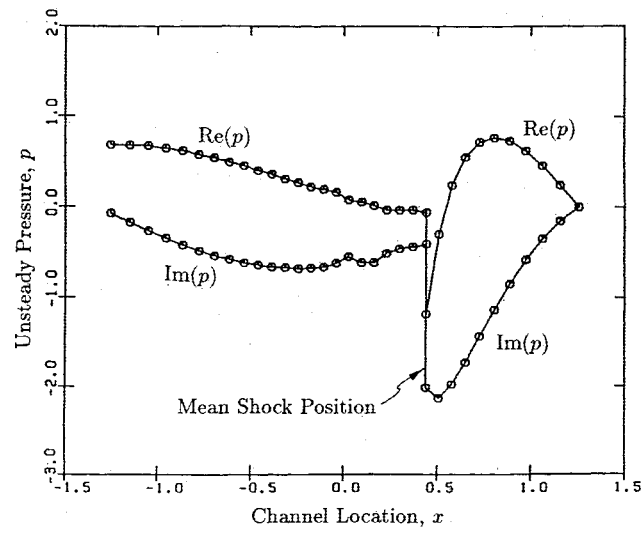

Fig. 4 Unsteady pressure on lower wall of hyperbolic channel for upstream variation in total pressure and density. The reduced frequency of excitation $\bar{\omega}$ is 4.665.

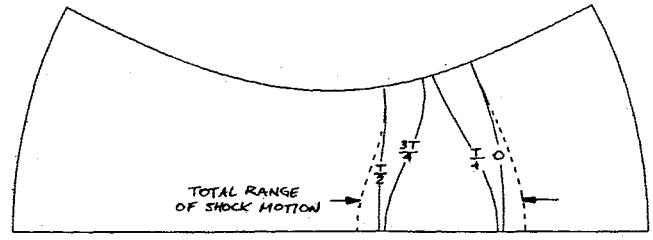

Fig. 5 Unsteady shock motion at four times during harmonic cycle. Note that upper portion of shock leads lower part. The reduced frequency $\bar{\omega}$ is 4.665.

Gostelow[37] using a conformal transformation technique. The unsteady incompressible flow has been analyzed by Atassi and Akai[3,4] using a semi-analytical technique. Therefore, since steady and unsteady solutions exist for this geometry, it is a useful test case with which to evaluate the present linearized Euler method. First, the steady flow through the cascade will be calculated using the present method. Then two different

unsteady flows will be examined. These include unsteady flows excited by torsional blade vibrations and those excited by an incident vortical and entropic gust.

The cascade has a pitch to chord ratio G of 0.99015, and a stagger angle ξ or 37.5 deg. An 80×16 node H-grid was generated for a single blade passage using a mixed algebraic and elliptic grid generator.[38] The boundary conditions for the steady flow are as follows. Upstream of the cascade the total pressure and density are specified to be unity. The incoming flow angle is specified to be 53.5 deg with respect to the axial direction or 16 deg with respect to the blade chord. Downstream, the static pressure is 0.98. This corresponds to a downstream Mach number of 0.170. The Newton solver was used to calculate the steady flow. Because the flow is compressible, the computed solution cannot be directly compared to the analytical incompressible solution of Gostelow.[37] However, using the Prandtl-Glauert transformation, the computed solution can be modified so that it more closely approximates the incompressible solution. The result is shown in Fig. 6 along with the analytical solution of Gostelow. Note the excellent agreement between the two solutions. Because the flow is nominally isentropic, the total pressure should be 1.0 throughout the domain. Because of truncation error in the numerical method, however, there is some variation in the computed total pressure. The maximum total pressure error for this case is about 0.01.

Having calculated the mean flow in the cascade, two unsteady flows now will be considered. In the first case, the unsteady flow is induced by blade vibration. The blades are assumed to vibrate in torsion about their midchords with a reduced frequency $\bar{\omega}$ of 0.40, based on chord and upstream velocity and an interblade phase angle σ of π. The calculated unsteady pressure distribution on the surface of the airfoils is shown in Fig. 7. Because of the difficulty in implementing the mean flow gradient terms used to extrapolate the boundary conditions from the mean blade location to the instantaneous blade location, these terms were "switched off" in the present analysis. This example also was analyzed by Atassi and Akai[3] using a semi-analytical technique that they developed to analyze incompressible flows. Their results are also shown in Fig. 7. Note the generally good agreement between the present method and the results of Atassi and Akai.

Atassi and Akai later included the mean flow gradient terms in their analysis[4] and demonstrated that the predicted unsteady aerodynamic loads on moving airfoils are strongly influenced by the large mean flow gradients at the leading and trailing edges. Hence, these terms should be included in the linearized Euler analysis.

In the next example, the response of the Gostelow cascade to a vortical gust is considered. Upstream of the rotor there may be some obstructions in the nonrotating frame that cause an approximately sinusoidal defect in the velocity. In the nonrotating frame, the flow is parallel and steady, and the pressure and total enthalpy are uniform. In the rotating frame, however, the flow is unsteady. The blades see a sinusoidally varying inlet velocity and, hence, feel an unsteady load. For this example it is assumed that the sinusoidal variation in the axial velocity has a wavelength of 4 blade pitches. This corresponds to an interblade phase angle σ of $-\pi/2$. Furthermore, the velocity in the circumferential direction in the nonrotating frame is zero. Hence, the circumferential component of velocity V in the rotating frame is due entirely to the rotational speed of the rotor. The unsteadiness that the moving blades see occurs at a frequency of $\omega = -\sigma V/G$. For the case considered here, this corresponds to a reduced frequency of 1.275. Time $t = 0$ is defined as the time at which the maximum velocity deficit would arrive at the leading edge of the reference blade if the cascade did not alter the incoming flow.

The unsteady linearized Euler code, which was run on an Alliant FX/8 computer, required about 8 min of CPU time. Shown in Fig. 8 are the real and imaginary parts of the

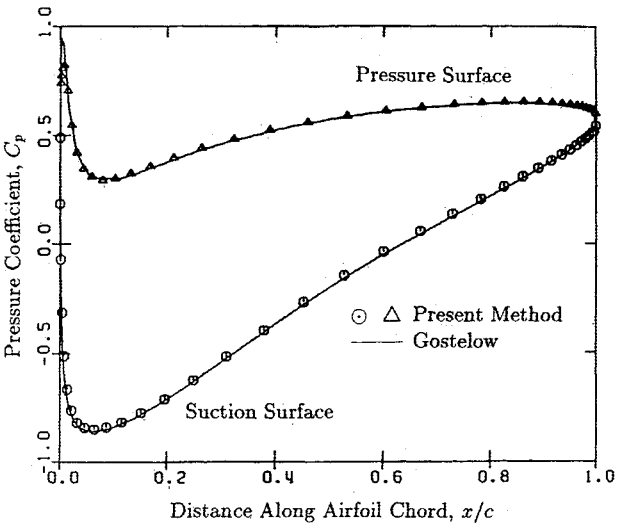

Fig. 6 Pressure along surface of airfoil. The Prandtl-Glauert correction was used to convert the calculated compressible flow pressure coefficient to the incompressible equivalent.

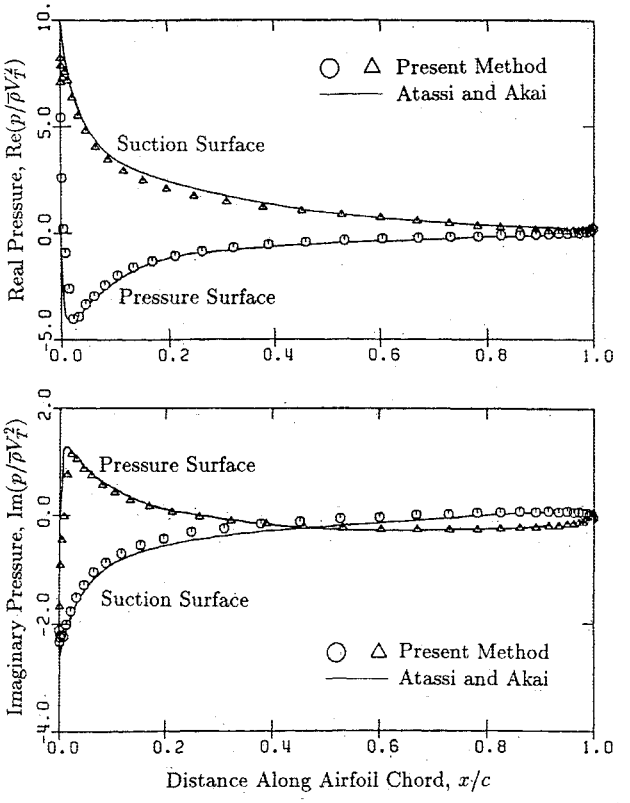

Fig. 7 Real and imaginary parts of unsteady pressure on the surface of a pitching airfoil. Reduced frequency $\bar{\omega} = 0.4$, interblade phase angle $\sigma = \pi$.

calculated unsteady pressure distribution. By integrating these pressures over the airfoil surface, one can obtain the unsteady lift and moment felt by each blade due to the inlet distortion. Also shown for comparison is the first harmonic component of the unsteady pressure as calculated by Giles using the program UNSFLO.[21,22] Giles' code is unique in that under the right conditions a time-space transformation allows the time-accurate flowfield to be represented in a single blade passage. At low Mach numbers and low interblade phase angles, however, more than one blade passage may be needed in the calculation. For this particular example, four blade passages were required. The grid used by Giles was, therefore, fairly large with 125×100 nodes. Eight periods were calculated so as

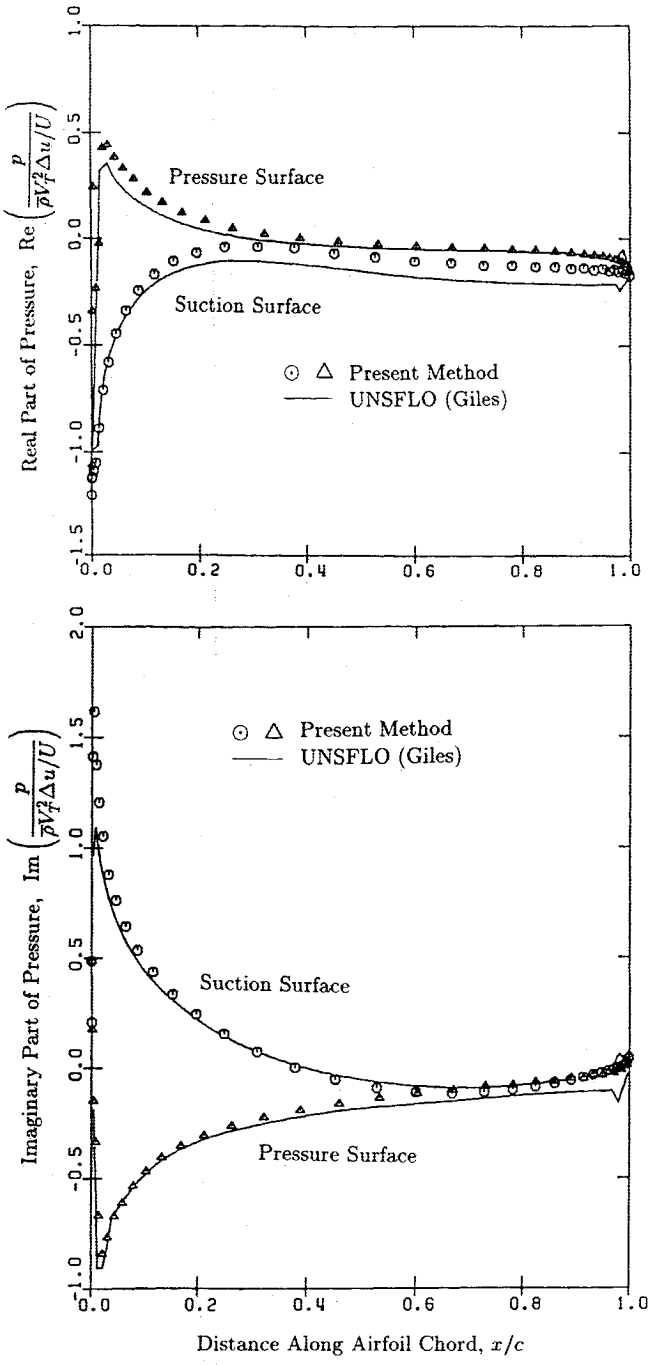

Fig. 8 Real and imaginary parts of nondimensional pressure on airfoil surface due to incoming vortical and entropic gust. The interblade phase angle σ is $-\pi/2$, the reduced frequency $\bar{\omega}$ is 1.275.

to reach a periodic state. This required about 8 h of computer time on an Alliant FX/8 computer. The time history of the computed pressure distribution was Fourier transformed so that the results could be compared directly to the present method. Note that the agreement is good, although not exact. At the present time, it is not clear what is causing these differences. However, considering the good qualitative agreement and the fact that the present method required a factor of 60 less CPU time, the preliminary results of the linearized Euler analysis are quite encouraging.

Concluding Remarks

In this paper, a method for predicting unsteady transonic flows in turbomachines has been presented. Such an analysis is useful for modeling the aeroelastic behavior of turbomachinery blading operating at transonic speeds. The method is based on the linearized Euler equations and fully accounts for the effects of mean blade loading, blade geometry, shock motion, and wake motion. Unlike linearized potential methods, the present method accounts for the generation of vorticity and entropy at shocks. Steady and unsteady entropy changes across shocks can have a profound influence on the motion of shocks and, hence, the present method should provide significantly better predictions for unsteady flows containing strong shocks or subject to low-frequency excitations.

To determine the steady flow, a Newton-iteration procedure is used that reduces the problem of solving the nonlinear Euler equations to one of solving a series of linearized equations, each similar to the linearized unsteady equations. The steady linearized Euler equations are discretized on a computational grid and solved directly. The Newton-iteration procedure converges very quickly with typical subsonic flow problems converging in about five iterations, whereas transonic problems may require up to 10 iterations. In addition, the similarity of the Newton-iteration equations to the linearized unsteady equations greatly simplifies the effort required to develop both a steady and an unsteady Euler code. In fact, many parts of the two codes are nearly identical.

Another important feature of the present analysis is the use of steady and unsteady shock and wake fitting. Shocks and wakes are modeled as discontinuities with jump conditions applied at the shock and wake surfaces. For steady flow calculations, shock fitting provides an accurate prediction of the shock position without the use of excessively fine grids. Fairly coarse grids can produce surprisingly good predictions of shock positions. But more importantly, the accuracy of the steady solution will affect the accuracy of the unsteady solution. Hence, the precise modeling of shocks obtained using shock fitting is essential if one is to accurately predict shock motions and, in turn, the unsteady aerodynamic loads on transonic airfoils.

Although the present work has demonstrated some of the advantages that the linearized Euler method offers in analyzing unsteady transonic flows, some issues still need to be resolved before the method can be successfully applied in aeroelastic analyses of transonic cascades. The major issue is the fitting of shocks. The shock-fitting algorithm presented in this paper requires that the shock be aligned with a computational grid line on a logically rectangular grid. This restricts the shock geometries that can be analyzed to normal shocks on fairly unskewed grids. Therefore, transonic flows through staggered cascades cannot be analyzed at the present time.

Acknowledgments

This work was performed at the Gas Turbine Laboratory of the Massachusetts Institute of Technology and was supported by NASA Lewis Research Center under grant number NSG 3079, with Dr. John Adamczyk, Dr. Donald Boldman, and Dr. Daniel Hoyniak serving as technical monitors. Additional support was provided by the Aircraft Engine Business Group of the General Electric Company and the Alison Gas Turbine Operations of the General Motors Corporation. This paper was prepared at United Technologies Research Center. The author gratefully acknowledges the generous support of the Fannie and John Hertz Foundation. The authors wish to express their gratitude to Dr. Joseph Verdon for his guidance throughout the course of this effort, and to Professor Michael Giles for providing both technical advice and a test case that appears in this paper.

References

[1]Whitehead, D. S., "Force and Moment Coefficients for Vibrating Aerofoils in Cascade," Aeronautical Research Council, London, Reports and Memoranda 3254, Feb. 1960.

[2]Whitehead, D. S., "Bending Flutter of Unstalled Cascade Blades at Finite Deflection," Aeronautical Research Council, London, Reports and Memoranda 3386, Oct. 1962.

[3]Atassi, H. and Akai, T. J., "Aerodynamic Force and Moment on Oscillating Airfoils in Cascade," American Society of Mechanical Engineers, New York, Paper 78-GT-181, April 1978.

[4]Atassi, H. and Akai, T. J., "Aerodynamic and Aeroelastic Characteristics of Oscillating Loaded Cascades at Low Mach Number. Part I: Pressure Distribution, Forces, and Moments," *Transactions of the ASME: Journal of Engineering for Power,* Vol. 102, No. 2, April 1980, pp. 344-351.

[5]Lane, F. and Friedman, M., "Theoretical Investigation of Subsonic Oscillatory Blade-Row Aerodynamics," NACA TN 4136, Feb. 1958.

[6]Whitehead, D. S., "Vibration and Sound Generation in a Cascade of Flat Plates in Subsonic Flow," Aeronautical Research Council, London, Reports and Memoranda 3685, Feb. 1970.

[7]Smith, S. N., "Discrete Frequency Sound Generation in Axial Flow Turbomachines," Aeronautical Research Council, London, Reports and Memoranda 3709, March 1972.

[8]Verdon, J. M., "The Unsteady Aerodynamics of a Finite Supersonic Cascade with Subsonic Axial Flow," *Transactions of the ASME: Journal of Applied Mechanics,* Vol. 40, No. 3, Sept. 1973, pp. 667-671.

[9]Verdon, J. M. and McCune, J. E., "Unsteady Supersonic Cascade in Subsonic Axial Flow," *AIAA Journal,* Vol. 13, Feb. 1975, pp. 193-201.

[10]Nagashima, T. and Whitehead, D. S., "Linearized Supersonic Unsteady Flow in Cascades," Aeronautical Research Council, London, Reports and Memoranda 3811, Feb. 1977.

[11]Adamczyk, J. J. and Goldstein, M. E., "Unsteady Flow in a Supersonic Cascade with Subsonic Leading-Edge Locus," *AIAA Journal,* Vol. 16, Dec. 1978, pp. 1248-1254.

[12]Bendiksen, O. O., "Bending-Torsion Flutter in Supersonic Cascades," *AIAA Journal,* Vol. 19, June 1981, pp. 774-781.

[13]Bendiksen, O. O., "Role of Shocks in Transonic/Supersonic Compressor Flutter," *AIAA Journal,* Vol. 24, July 1986, pp. 1179-1186.

[14]Goldstein, M. E., Braun, W., and Adamczyk, J. J., "Unsteady Flow in a Supersonic Cascade with Strong In-Passage Shocks," *Journal of Fluid Mechanics,* Vol. 83, Pt. 3, 1977, pp. 569-604.

[15]Verdon, J. M. and Caspar, J. R., "Subsonic Flow Past an Oscillating Cascade with Finite Mean Flow Deflection," *AIAA Journal,* Vol. 18, May 1980, pp. 540-548.

[16]Carta, F. O., "Unsteady Gapwise Periodicity of Oscillating Cascaded Airfoils," American Society of Mechanical Engineers, New York, Paper 82-GT-286, April 1982.

[17]Whitehead, D. S., "Force and Moment Coefficients for High Deflection Cascades," Univ. of Cambridge, Dept. of Engineering, Cambridge, England, CUED/A-Turbo/TR 98, May 1980.

[18]Verdon, J. M. and Caspar, J. R., "A Linearized Unsteady Aerodynamic Analysis for Transonic Flows," *Journal of Fluid Mechanics,* Vol. 149, Dec. 1984, pp. 403-429.

[19]Whitehead, D. S., "The Calculation of Steady and Unsteady Transonic Flow in Cascades," Univ. of Cambridge, Dept. of Engineering, Cambridge, England, CUED/A-Turbo/TR 118, 1982.

[20]Ni, R. H. and Sisto, F., "Numerical Computation of Nonstationary Aerodynamics of Flat Plate Cascades in Compressible Flow," *Transactions of the ASME: Journal of Engineering for Power,* Vol. 98, April 1976, pp. 165-170.

[21]Giles, M. B., "UNSFLO: A Numerical Method for Unsteady Inviscid Flow in Turbomachinery," Massachusetts Inst. of Technology, Cambridge, MA, TR CFDL-TR-86-6, Dec. 1986.

[22]Giles, M. B., "Calculation of Unsteady Wake/Rotor Interactions," AIAA Paper 87-0006, Jan. 1987.

[23]Ni, R. H., "A Multiple-Grid Scheme for Solving the Euler Equations," *AIAA Journal,* Vol. 20, 1982, pp. 1565-1571.

[24]Giles, M. B., "Newton Solution of Steady Two-Dimensional Transonic Flows," Ph.D. Thesis, Massachusetts Inst. of Technology, Cambridge, MA, June 1985.

[25]Drela, M., "Two-Dimensional Transonic Aerodynamic Design and Analysis Using the Euler Equations," Massachusetts Inst. of Technology, Cambridge, MA, Gas Turbine Lab. Rept. 187, Feb. 1986.

[26]Hall, K. C., "A Linearized Euler Analysis of Unsteady Flows in Turbomachinery," Sc.D. Thesis, Massachusetts Inst. of Technology, Cambridge, MA, May 1987.

[27]Moretti, G., "Floating Shock Fitting Technique for Imbedded Shocks in Unsteady Multidimensional Flows," *Proceedings of the 1974 Heat Transfer and Fluid Mechanics Institute,* Stanford Univ. Press, Stanford, CA, 1974, pp. 184-201.

[28]Moretti, G., "Circumspect Exploration of Multidimensional Imbedded Shocks," *AIAA Journal,* Vol. 14, July 1976, pp. 894-899.

[29]Verdon, J. M., Adamczyk, J. J., and Caspar, J. R., "Subsonic Flow Past an Oscillating Cascade with Steady Blade Loading—Basic Formulation," *Unsteady Aerodynamics,* edited by R. B. Kinney, Univ. of Arizona, Tucson, AZ, July 1975, pp. 827-851.

[30]Verdon, J. M., "Linearized Unsteady Aerodynamic Theory," United Technologies Research Center, East Hartford, CT, UTRC Rept. R85-151774-1, Nov. 1985.

[31]Giles, M. B., "Non-Reflecting Boundary Conditions for the Euler Equations," Massachusetts Inst. of Technology, Cambridge, MA, TR CFDL-TR-87-1, Feb. 1987.

[32]Berry, P. E., "Computation of Unsteady Flow in a Blade Passage," *Unsteady Aerodynamics of Turbomachines and Propellers,* Cambridge Univ., Dept. of Engineering, Cambridge, England, Sept. 1984, pp. 191-203.

[33]Engquist, B. and Majda, A., "Absorbing Boundary Conditions for the Numerical Simulation of Waves," *Mathematics of Computation,* Vol. 31, No. 139, July 1977, pp. 629-651.

[34]Emmons, H. W., "The Numerical Solution of Compressible Fluid Flow Problems," NACA TN 932, May 1944.

[35]Emmons, H. W., "The Theoretical Flow of a Frictionless, Adiabatic, Perfect Gas Inside of a Two-Dimensional Hyperbolic Nozzle," NACA TN 1003, May 1946.

[36]Park, M. and Caughey, D. A., "Transonic Potential Flow in Hyperbolic Nozzles," *AIAA Journal,* Vol. 24, June 1986, pp. 1037-1039.

[37]Gostelow, J. P., *Cascade Aerodynamics,* Pergamon Press, New York, 1984, Chap. 5.

[38]Thompson, J. F., Thames, F. C., and Mastin, W., "A Code for Numerical Generation of Boundary-Fitted Curvilinear Coordinate Systems on Fields Containing any Number of Arbitrary Two-Dimensional Bodies," *Journal of Computational Physics,* Vol. 24, No. 3, 1977, pp. 274-302.